Astronomy & Astrophysics

Observations of CO on Saturn and Uranus at millimeter wavelengths: new upper limit determinations

T. Cavalié[1], F. Billebaud[1], T. Fouchet[2], E. Lellouch[2], J. Brillet[1], and M. Dobrijevic[1]

[1] Université Bordeaux I, CNRS, Observatoire Aquitain des Sciences de l'Univers, Laboratoire d'Astrophysique de Bordeaux, 2 rue de l'Observatoire, BP 89, 33270 Floirac, France
e-mail: cavalie@obs.u-bordeaux1.fr
[2] Observatoire de Paris-Meudon, Laboratoire d'Études Spatiales et d'Instrumentation en Astrophysique, France

ABSTRACT

Aims. We observed Saturn and Uranus at CO millimetric line wavelengths in order to better constrain the origin of CO in the atmospheres of these planets. CO sources can be either of internal or of external origin.
Methods. We recorded broad multi-band spectra of Saturn and Uranus at the frequencies of the $J = 1 \rightarrow 0$ and $J = 2 \rightarrow 1$ CO lines.
Results. As we do not detect any CO line in the spectra, we derive new upper limits of the abundance of CO in the atmospheres of Saturn and Uranus. The value we obtain for Saturn (6.3×10^{-8}, restricted to the stratosphere) is larger than the value of the CO mixing ratio in the external origin model used. New observations with higher sensitivity and/or longer observing time should enable us to determine the CO external source strength. The upper limit we derive on Uranus is slightly lower (2.7×10^{-8}, restricted to the stratosphere) than the value derived from an early observation of CO on Uranus, at infrared wavelength. As the fluorescence model used then did not take scattering effects into account, we suggest that the value could be overestimated.

Key words. planets and satellites: individual: Saturn, Uranus – radio lines: solar system

1. Introduction

Water and carbon dioxide have been detected in the stratospheres of the four giant planets and Titan (Feuchtgruber et al. 1997, 1999; Coustenis et al. 1998; Burgdorf et al. 2006). The presence of these condensable species above the tropopause cold trap (except CO_2, which does not condense on Jupiter and Saturn) implies the presence of an external supply of oxygen. Different possible sources have been proposed: infall of interplanetary dust particles (IDPs), sputtering from the planetary rings and icy satellites, or massive impacts of kilometer-sized comets or asteroids (Moses et al. 2000).

Different techniques can be used to discriminate between these various sources. First, the spatial distribution (altitude and latitude) of oxygenated compounds can trace localized inputs. Lellouch et al. (2002) showed that the water in Jupiter is restricted to pressure levels higher than the 0.5-mbar level and that CO_2 is enhanced in the southern hemisphere: both species must then originate from localized, recent events: the Shoemaker Levy 9 (SL9) impacts. A recent analysis of submillimeter spectra of Odin and SWAS (Submillimeter Wave Astronomy Satellite) space telescopes seems to confirm the cometary origin of the stratospheric water on Jupiter (Cavalié et al. 2008). A second possibility is to determine which chemical species, water or a species with a C−O bond (CO, CO_2, ...), is the main oxygen carrier to the stratospheres of the giant planets. From observations in the millimetric range or at 5-μm, Bézard et al. (2002) and Lellouch et al. (2002, 2005) have measured the CO abundance in the stratospheres of Jupiter and Neptune, and demonstrated that the ratios of the CO to the H_2O deposition rates are larger than 30 and can be as large as 200. These large CO/H_2O ratios strongly favor large impacts as the main source of oxygen in the

stratospheres of Jupiter and Neptune, as shown by SL9 (Lellouch 1996; Moses 1996; Moses et al. 2000).

In between, the situation of Saturn and Uranus is still unclear, because the CO mixing ratio in the stratospheres of these planets is still unknown or uncertain, and also since the CO origin cannot definitely be attributed to an external flux. Indeed, an internal source of CO also exists in giant planets in the form of convective transport from the deep warm atmosphere where the equilibrium CO abundance is higher than in the shallow atmosphere. This internal source is observed on Jupiter and Neptune (Bézard et al. 2002; Lellouch et al. 2005). Its measurement could be very useful to constrain the O/H ratio and the convective activity in the giant planet deep interiors (Bézard et al. 2002).

On Saturn, CO has been detected from 5-μm spectroscopy at a level of 1 ppb (if uniformly mixed) by Noll & Larson (1991) but the authors were not able to independently measure the stratospheric and tropospheric mixing ratios. Therefore it is not possible to reliably estimate the relative contributions of the external and internal flux. Later, Rosenqvist et al. (1992) could only derive an upper limit of 1×10^{-7} from their observations at millimeter wavelengths. On Uranus, CO has been detected at 5-μm (Encrenaz et al. 2004) from fluorescent emission. These authors derived a stratospheric mixing ratio of 3×10^{-8} but within an uncertainty of a factor of two. In the troposphere, they derived an upper limit of 2×10^{-8}. The latter improved the previous upper limits from Marten et al. (1993) and Encrenaz et al. (1996), which were $\sim 3 \times 10^{-8}$ and 5×10^{-7} respectively. The large error bars in Encrenaz et al. (2004) did not allow the authors to distinguish the external from the internal flux. For Uranus again, the CO/H_2O deposition rate ratio could not be measured, and the origin of the external oxygen remains

unconstrained. We present new observations to help constrain the abundance of CO in the atmospheres of Saturn and Uranus.

Our observations are described in Sect. 2. The radiative transfer model is presented in Sect. 3 and we show our results in Sect. 4. Discussion and conclusions are given in Sect. 5.

2. Observations

We observed Saturn and Uranus on 16−18 September 2006 with the Institut de RadioAstronomie Millimétrique (IRAM) 30-m telescope, at Pico Veleta, Spain. The angular sizes of the planets were 16.6 arcsec for Saturn and 3.7 arcsec for Uranus. The Sub-Earth Point latitudes were respectively −14.3° and −5.25° for Saturn and Uranus.

We simultaneously used two receivers (A and B) which share two backends at 1 and 3-mm wavelength in order to observe the CO $J = 1 \rightarrow 0$ and $J = 2 \rightarrow 1$ lines at 115.271 GHz and 230.538 GHz. Each receiver covers a bandwidth of 512 MHz at 115 GHz and 1024 MHz at 230 GHz. Both receiver spectral resolutions were set at 1 MHz. The receivers were operated in a single side band mode. The side band rejection was 0.001 at 115 GHz and 0.01 at 230 GHz. The wobbler switching technique was used and the wobbler frequency was set to 0.5 Hz. System temperatures ranged from 320 K to 430 K during the first night (from 380 K to 500 K during the second night) on the 1-mm band and from 250 K to 420 K during the first night (from 260 K to 400 K during the second night) on the 3-mm band. The zenithal atmospheric opacity value was about 0.15−0.20 at 115 GHz and 0.25−0.30 at 230 GHz. A large absorption feature appears at 231.280 GHz on Uranus and Saturn spectra (see Figs. 1 and 2). This line is the terrestrial ozone line.

On Saturn and Uranus, the expected CO tropospheric/low stratospheric absorptions are broad; they cover several GHz in frequency. This is the reason why we adopted the observation technique that is described in Lellouch et al. (2005) to observe these lines. This technique consists of using both receivers A and B in parallel in order to cover the widest band available: by taking an overlap of 1/4 of the bands (128 MHz at 115 GHz and 256 MHz at 230 GHz), it is possible to cover 896 MHz and 1792 MHz for one single tuning at the CO(1−0) and CO(2−1) frequencies. For Saturn and Uranus, we covered 1280 MHz at 115 GHz and 4096 MHz at 230 GHz (see Figs. 1 and 2). All the tunings were observed from 1/2 h to 1 h in a cyclic scheme.

At 115 GHz, 3 contiguous spectra were obtained, while we observed 5 spectral bands around 230 GHz. The intense terrestrial O_2 atmospheric absorption around 118.750 GHz prevents ground-based observations rightwards of 115.5 GHz. This is the reason why we only have 3 bands at 115 GHz, respectively centered around 115.271 GHz, 114.887 GHz and 114.503 GHz. The 115 GHz spectrum was not probed over 115.5 GHz.

Once all the observations were carried out, the individual spectra were connected. As two contiguous spectra generally did not have the same continuum level, we averaged the spectra in their overlap part and rescaled them one to another. So, all the spectra have been rescaled according to the continuum of the first spectrum of each band. The final spectrum frequency ranges are 114.263−115.511 GHz and 228.504−232.568 GHz. Finally, the spectra were reduced as for classical spectra. After removing a polynomial baseline of maximum degree 3, we removed the ripples with the greatest amplitude with a FFT procedure. The ripple frequencies that were removed were the ones present on each spectrum (at 115 GHz and 230 GHz, for Saturn and Uranus). As we performed no absolute calibration, the lines
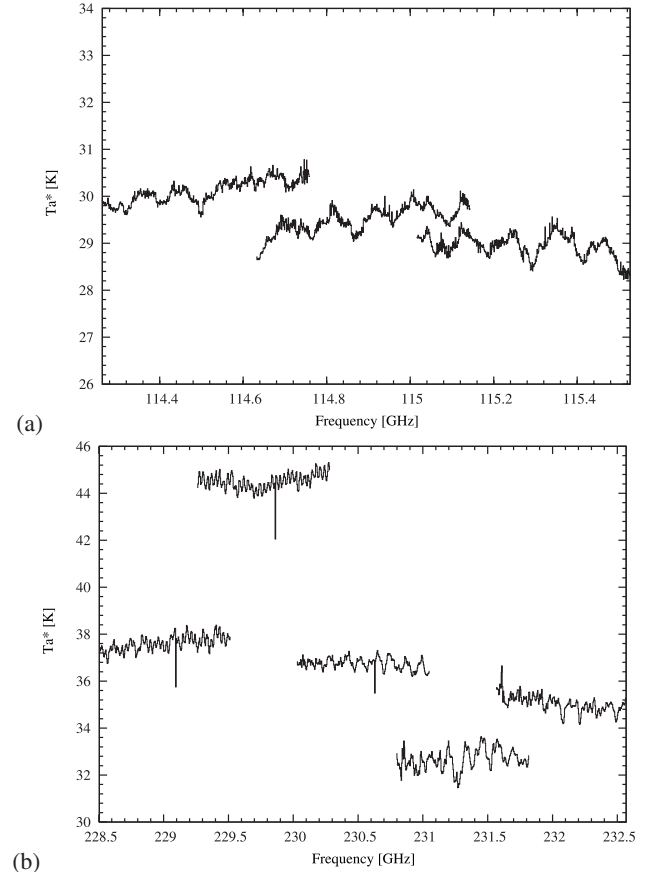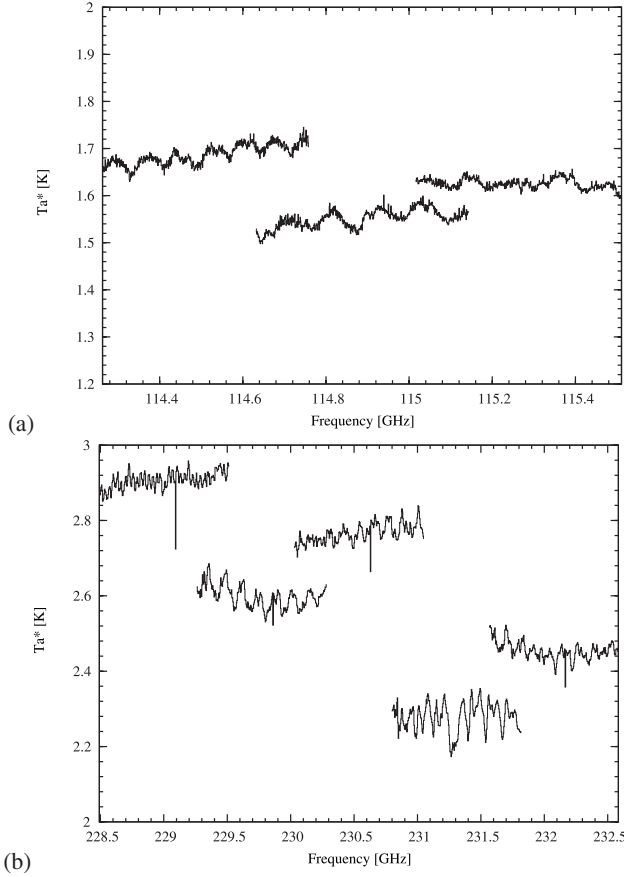

Fig. 1. Spectra of Saturn at **a)** 115 GHz and **b)** 230 GHz in the antenna temperature scale. Receiver A has a corrupt channel. It can be seen in the middle of the first three lowest frequency bands at 230 GHz. This channel is removed before reducing the spectra. The terrestrial ozone absorption band can be seen at 231.280 GHz. This feature is not taken into account when computing the spectrum noise level.

were interpreted in terms of line to continuum ratios. All the lines were smoothed to a 16 MHz spectral resolution in order to reduce the noise level. The 3-σ levels we obtain, depending on the continuum value, are shonw in Table 1. The best 3-σ level we obtain are for the CO(2−1) line at 230 GHz either on Saturn or Uranus, after converting the antenna temperature noise level intensity of each spectrum into a brightness temperature noise level intensity.

3. Radiative transfer

We modeled the observed millimetric radiation with a line-by-line non-scattering radiative transfer model. We computed synthetic spectra in the wavelength ranges of the CO(1−0) and (2−1) lines. The program respects the approximate spherical geometry of the planets (except the rings on Saturn) so that planetary disk and limb contributions were taken into account. We assumed a uniform distribution of all opacity sources and, for simplicity, we adopted mean thermal profiles for both planets since our beam size is comparable to or larger than the planetary disks. Thus, the total opacity on a line of sight only depends on the total thickness of the atmosphere on this line of sight. Therefore, we have a symmetry, in terms of opacity sources and temperature distributions, around the central point of the disk. This is why we only computed synthetic spectra for a given number of points located on the planetary disk

(a)

(b)

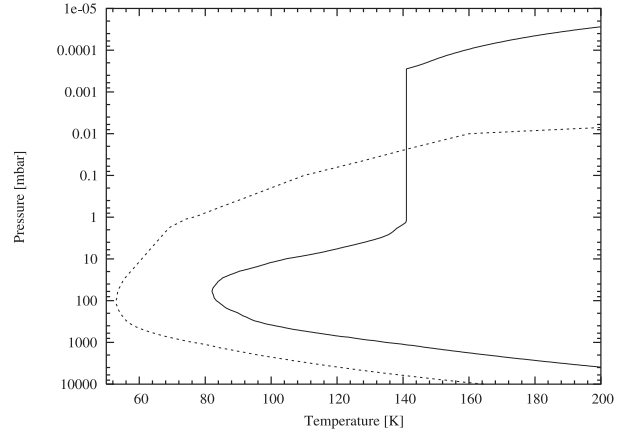**Fig. 2.** Spectra of Uranus at **c)** 115 GHz and **d)** 230 GHz. Same caption as Fig. 1.

Fig. 3. Thermal profiles of Saturn (solid line) and Uranus (dashed line).

Fig. 4. Ammonia, phosphine and carbon monoxide mixing ratio vertical profiles on Saturn, all in solid lines. The internal and external source of CO models come from Noll & Larson (1991) (N&L'91 on the plot). The upper limits we have derived for the internal source (dotted lines) and for the external source (dashed lines) are also displayed.

Table 1. Continuum and 3-σ noise level in the antenna temperature scale on the CO(1−0) and CO(2−1) spectral bands.

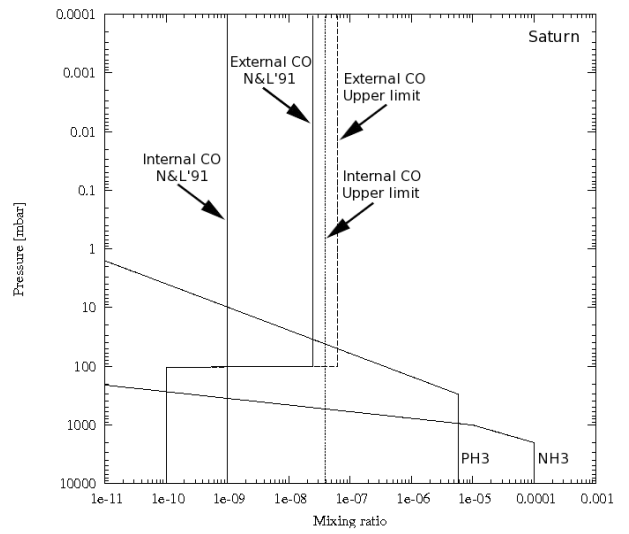| T_a^*	115 GHz		230 GHz	
	continuum	3-σ	continuum	3-σ
Saturn	30.1 K	213 mK	37.5 K	420 mK
Uranus	1.65 K	9 mK	2.9 K	33 mK

radius. Assuming local thermal equilibrium, the specific intensity $I_\nu \left[\text{W m}^{-2} \text{ sr}^{-1} \text{ Hz}^{-1} \right]$ along a given line of sight is:

$$I_\nu = \int_0^{\tau_\nu(\infty)} B_\nu(T(z)) e^{-\tau_\nu} d\tau_\nu. \tag{1}$$

The parameter τ_ν is the optical depth, $B_\nu(T)$ is the Planck function and $T(z)$ is the atmospheric vertical thermal profile. The thermal profiles we used come, from Ollivier et al. (2000) for Saturn and from Lindal (1992) for the troposphere and Orton et al. (1987) for the stratosphere for Uranus (see Fig. 3). Continuum opacity is dominated by H_2-He-CH_4 collision-induced absorption (Borysow et al. 1985; Borysow & Frommhold 1986; Borysow et al. 1988). Following Moreno (1998), the opacity due to the far wings of ammonia and phosphine lines is also included (only NH_3 in the case of Uranus). We used the Davis et al. (1996) ammonia and Fletcher et al. (2007) phosphine mixing ratio vertical profiles for Saturn. The mixing ratio profile of ammonia on Uranus is in agreement with Hofstadter & Muhleman (1989) measurements ($q_{NH_3} = 7.8 \times 10^{-7}$ below the condensation level).

We tested the CO mixing ratio vertical profiles inferred by Noll & Larson (1991) for the atmosphere of Saturn. The first one is based on an internal source of CO (1 ppb, constant with altitude), while the other is the signature of an external supply of CO (2.5×10^{-8} in the stratosphere and 10^{-10} in the troposphere). For Uranus, the CO lines were computed from the Encrenaz et al. (2004) models. The authors tentatively favored an external origin for CO (3×10^{-8} above the 100 mbar level) and set an upper limit on the magnitude of a tropospheric source (vertical profile with 2×10^{-8} constant with altitude). Our 3-σ mixing ratio values are discussed in Sect. 4. All these profiles are shown in Figs. 4 and 5.

Spectroscopic parameters for NH_3, PH_3 and CO were taken from Pickett et al. (1998). The line widths are determined by the collisional line widths for H_2 and He broadening. The broadening γ and temperature dependence exponent n values we took for NH_3, PH_3 and CO are summarized in Table 2. All lines, except the NH_3 ones, are assumed to be Voigt-shaped. Following Moreno (1998), we take a modified Van Vleck and Weisskopf line profile for ammonia.

We performed our analysis in terms of line to continuum ratios. We compared our continuum model to previously
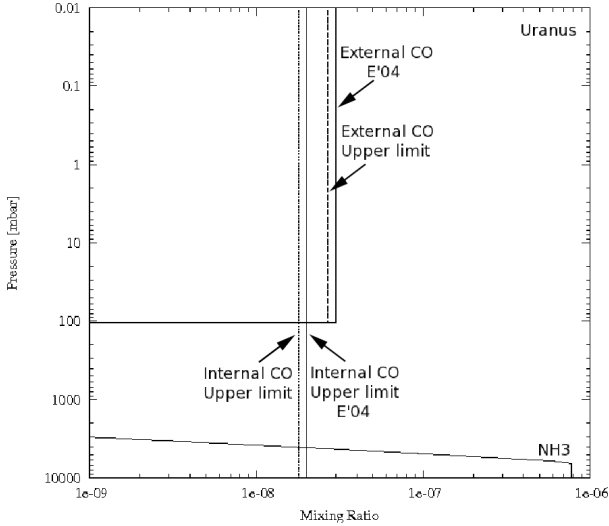
Fig. 5. Ammonia and carbon monoxide mixing ratio vertical profiles on Uranus, all in solid lines. Both CO internal (upper limit) and external (best fit model) origin profiles come from Encrenaz et al. (2004) (E'04 on the plot). Our upper limits are plotted in dotted lines for the internal source and in dashed lines for the external source.

Table 2. Collisional line width γ [cm^{-1} atm^{-1}] (at 300 K) and temperature dependence factor n for NH$_3$, PH$_3$ and CO with H$_2$ and He and for Saturn and Uranus (a blank space means that no data is available).

γ	H$_2$	He	Saturn	Uranus
NH$_3$	0.069		0.069	0.069
PH$_3$ (1–0)	0.1078	0.0618	0.1011	0.1003
PH$_3$ (2–1)	0.1064	0.0606	0.0997	0.0990
CO (1–0)	0.0749	0.0479	0.0709	0.0696
CO (2–1)	0.0715	0.0468	0.0679	0.0666
n	H$_2$	He	Saturn	Uranus
NH$_3$	0.67		0.67	0.67
PH$_3$	0.73	0.30	0.67	0.66
CO (1–0) & (2–1)			0.60	0.60

References: Berge & Gulkis (1976) and Brown & Peterson (1994) for NH$_3$, Lévy et al. (1993) and Lévy et al. (1994) for PH$_3$ and Draegert & Dudley (1968), Varanasi (1988), Beaky et al. (1996) and Weisstein & Serabyn (1996) for CO.

published observations. On Saturn, the continuum disk brightness temperature of our model is 141.6 K at 115 GHz and 140.0 K at 230 GHz. These numbers are consistent with Klein et al. (1978) (~140 ± 15 K at 115 GHz and ~135 ± 11 K at 230 GHz). The good match of our continuum model to observations is confirmed with the Ulich (1981) data. The author reports a disk brightness temperature of 150 ± 7 K at 86 GHz and 164 ± 12 K at 142 GHz. As noted by the author, the observations at 142 GHz were carried out with a high inclination of the rings, increasing the apparent brightness temperature of the disk. With our model, we obtain 141.2 K at 86 GHz and 141.6 K at 142 GHz. At 310 GHz, our model gives 137.7 K, in agreement with Hildebrand et al. (1985). The disk brightness temperature we model for Uranus is 94.8 K at 200 GHz and 91.5 K at 230 GHz, consistent with Encrenaz et al. (1996) (T_B = 97.4 K at 200 GHz) and Orton et al. (1986) (T_B = 93.7 ± 3.0 K at 230 GHz).

Giant planets have rapid rotation periods. This induces a smearing of the lines which is linked to the rotation period and radius of the planets (see Table 3). Indeed, the radiation emitted along a line of sight are Doppler shifted because of the projected

Table 3. Saturn and Uranus physical characteristics (Lindal 1992; Conrath et al. 1987; Conrath & Gautier 2000; de Graauw et al. 1997; Baines et al. 1995).

|	Saturn	Uranus
Rotation period	10.2 h	17.9 h
Equatorial radius	60 268 km	25 559 km
Polar radius	54 364 km	24 973 km
H$_2$ molar fraction	0.8606	0.8320
He molar fraction	0.135	0.152
CH$_4$ molar fraction	4.4×10^{-3}	1.6×10^{-4}

velocity of the rotating gas. The smearing effect is maximum when the Sub-Earth Point latitude is close to 0°. To take this into account, the planetary disk was partitioned into a regular square grid. On each point of the grid, a synthetic spectrum is calculated by interpolating the spectra that were computed on a planetary disk radius. The spectra of the grid are then shifted in frequency, according to their location, and averaged with appropriate weights by taking the antenna pattern (2D Gaussian function) into account (Bergin et al. 2000; Lellouch et al. 2002). Although the CO lines are formed in the lower stratosphere, the lines appear to be in absorption, because the temperature where the line is formed is lower than the tropospheric continuum temperature. According to our model, we do not expect any observable stratospheric emission peak in the line core at 115 GHz and 230 GHz, unlike lines at higher frequencies (Cavalié et al. 2007). Because the lines are formed at high pressure levels, the CO lines are broad (Encrenaz et al. 1996). Thus, the smearing was found to have only a small effect on the final spectrum compared to the line width.

The rings of Saturn are sources of flux emission/absorption at millimeter wavelength (Dunn et al. 2005; de Pater & Dickel 1991). With a Sub-Earth Point latitude of −14.3° at the time of the observations, the rings hide ~10% of the northern part of the disk and add their own flux. This is why we pointed the telescope towards the planet between the southern limb and the rings. The contribution of the rings cannot be neglected when analysing submillimeter and infrared data. But Melnick et al. (1983) and de Pater & Dickel (1991) show that the brightness temperature of the rings (~20−30 K) is well below the temperature of the disk at 1-mm and 3-mm (~140 K). So the flux added by the ring contribution is not very important at these wavelengths. Therefore, we do not include the effect of the rings in our analysis. Moreover, as we do not analyse the data in terms of absolute intensities, we assume that the attenuation of the flux of the disk due to the rings does not change the result. Nevertheless, we pointed the telescope towards the mid-point of a segment going from the inner ring to the southern limb in order to have the maximum flux coming from the planet. This shift of the pointing on the planetary disk was taken into account when modeling the emission of the planet.

4. Analysis

The CO(1−0) and (2−1) lines are the weakest CO lines below 1000 GHz. Indeed, the tropopause temperature on Saturn and Uranus are 82 K and 53 K respectively, so that the population density of the energy levels peaks for higher frequency lines. However, the atmospheric opacity is lower at 115 GHz and 230 GHz than for higher frequencies. The best compromise at such low frequencies is reached at 230 GHz. This is why the upper limits come from the 230 GHz observation analysis. As a consequence of the broad width of the CO lines, we do not exactly reach the continuum in the 230 GHz spectrum of Saturn.
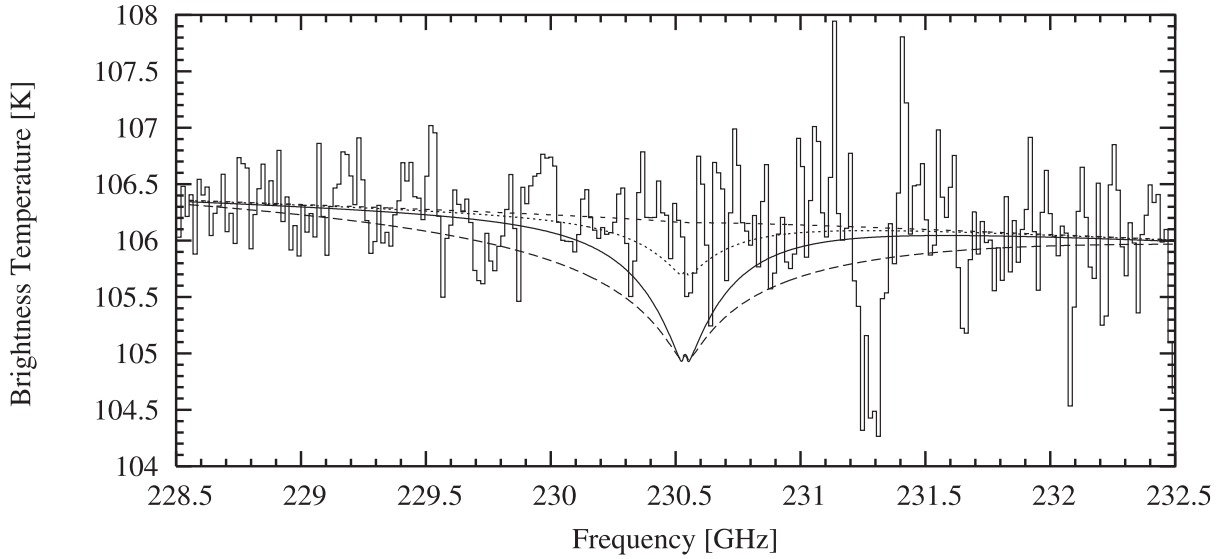
Fig. 6. Observed ^{12}CO (2−1) spectra on Saturn. The total bandwidth is 4 GHz and the spectral resolution is 16 MHz. The spectra resulting from the upper limits we derived are plotted as follows: our 3-σ upper limit of 6.3×10^{-8} in the stratosphere (external source of CO) in solid line and our 3-σ upper limit of 3.9×10^{-8} constant with altitude (internal source of CO) in long-dashed lines. The internal source of CO model (short-dashed lines) as well as the external source of CO (dotted lines) taken from Noll & Larson (1991) are also plotted for comparison with our upper limits. The absorption feature at 231.280 GHz is the terrestrial O$_3$ line.
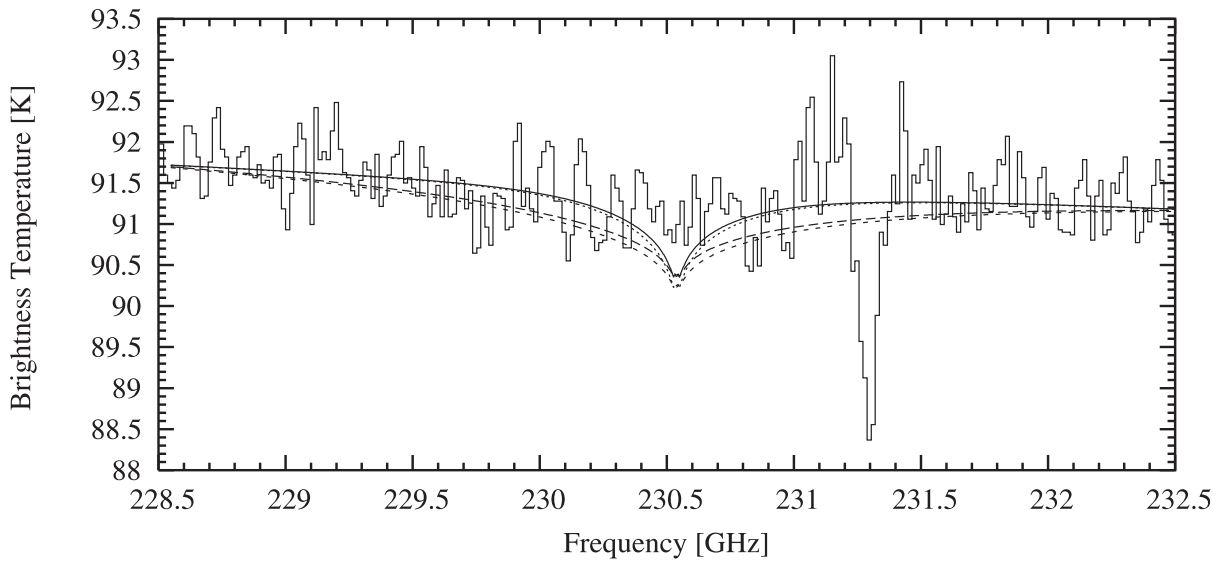
Fig. 7. Observed ^{12}CO (2−1) spectra on Uranus. The total bandwidth is 4 GHz and the spectral resolution is 16 MHz. The short-dashed lines correspond to the upper limit determined by Encrenaz et al. (2004) for a CO mixing ratio constant with altitude ($q_{CO} = 2 \times 10^{-8}$). The external source of CO model (dotted lines) is the Encrenaz et al. (2004) best fit model ($q_{CO} = 3 \times 10^{-8}$ restricted to the stratosphere). Our 3-σ upper limits are plotted in solid line ($q_{CO} = 2.7 \times 10^{-8}$, restricted to the stratosphere) and in long-dashed lines ($q_{CO} = 1.8 \times 10^{-8}$, constant with altitude). The absorption feature at 231.280 GHz is the terrestrial O$_3$ line.

Hence, the low frequency edges of the synthetic spectra have been rescaled to match the edge of the 3-σ model.

None of the CO lines we targeted were detected on Saturn or Uranus. From the 230 GHz observations of Saturn analysis, we derive a CO mixing ratio 3-σ upper limit of 3.9×10^{-8} for a constant mixing ratio of CO with altitude. This is an improvement by a factor of 3 compared to the Rosenqvist et al. (1992) measurement. However, this limit is well above the 1 ppb level of the internal origin model of Noll & Larson (1991). If the bulk of CO is restricted to the stratosphere, then we derive an upper limit for the CO mixing ratio of 6.3×10^{-8}. Once again this value is above

the Noll & Larson (1991) value in the stratosphere (2.5×10^{-8}), but only slightly. All the spectra discussed above are displayed in Fig. 6.

The observations of Uranus at 230 GHz (see Fig. 7) led to an upper limit of 1.8×10^{-8} for a mixing ratio constant with altitude (internal origin) and 2.7×10^{-8} if all the CO is in the stratosphere. The first value is consistent with the Encrenaz et al. (2004) upper limit for an internal source and the second one is consistent with the upper limit derived by Marten et al. (1993). However, the latter seems to be in contradiction with the Encrenaz et al. (2004) detection level in the stratosphere, at

face value. However, the authors mention that their fluorescence model could overestimate the CO abundance by at least a factor of 2.

5. Discussion

Observations of CO in the atmospheres of the giant planets are of key importance in order to determine the origin of oxygenated compounds that are present in their atmospheres. CO was first detected in the atmosphere of Saturn in 1985−1986. Noll et al. (1986) could not distinguish between an internal (q_{CO} = 1 ppb constant with altitude) and an external (q_{CO} = 2.5×10^{-8} restricted to the stratosphere) supply of atmospheric CO. From their 1990−2230 cm^{-1} high-resolution spectrum, Noll & Larson (1991) detected thirteen CO lines but were unable to firmly conclude on an internal origin, even if one of the lines favored an internal origin. From photochemical modeling, Moses et al. (2000) also could not distinguish between the origin scenarios, although both an internal and an external origin was favored as the simplest method to explain all the CO, CO_2 and H_2O observations. In their photochemical model of the atmosphere of Saturn, Ollivier et al. (2000) proposed a cometary-like composition for the oxygen external flux. This scenario cannot provide enough CO in the stratosphere of Saturn, so Ollivier et al. (2000) tentatively inferred that CO was mixed upward from the deep interior levels. Contrary to Ollivier et al. (2000), Moses et al. (2000) could not reproduce the CO_2 and H_2O data from ISO (Infrared space Observatory) with an influx of water alone and required some external influx of carbon-oxygen bonded species. The 3-σ upper limit of 3.9×10^{-8}, restricted to the stratosphere found here still cannot reject the external origin model from Noll & Larson (1991). It also cannot reject the external source model of Moses et al. (2000), where the CO mixing ratio increases with altitude and becomes greater than our upper limit between 10^{-1} and 10^{-5} mbar. Because the atmospheric layers above 10^{-1}–10^{-2} mbar do not contribute to the radiation at these wavelengths, the line is not sensitive to an increase of the CO mixing ratio in this part of the stratosphere. New observations with higher sensitivity and/or more observing time would be needed at this frequency (230 GHz) to reach the 2.5×10^{-8} level.

The weakness of the internal heat source in Uranus may be the cause of the limited convection in the deep interior of the planet (Hunten 1978; Wallace 1980), implying a lack of disequilibrium species, like CO, in its troposphere. Moreover, the quasi-isothermal structure of Uranus in the 1-mbar to 1-bar pressure range does not favor spectroscopic detection of minor constituents. The first attempts to detect CO at millimetric wavelengths led to upper limits on the mid-atmospheric (10-mbar) CO mixing ratio (4×10^{-8}, Rosenqvist et al. 1992; 3×10^{-8}, Marten et al. 1993). From CSO-FTS observations, Encrenaz et al. (1996) inferred an upper limit for the tropospheric content of CO (5×10^{-7}). The fluorescence of CO was detected in the atmosphere of Uranus by Encrenaz et al. (2004). Their atmospheric model suggests that the CO mixing ratio is greater in the stratosphere (3×10^{-8} if all CO is restricted to the stratosphere) than in the troposphere (upper limit: 2×10^{-8}). However, we did not detect the CO (2−1) line and a noise level analysis led to a 1.8×10^{-8} upper limit if the CO mixing ratio is constant with altitude (internal origin) and 2.7×10^{-8}, if restricted to the stratosphere (external origin). Our upper limit for the internal origin is consistent with the one derived by Encrenaz et al. (2004). However, our external origin upper limit is slightly lower than the Encrenaz et al. (2004) detection level. But, their model

did not take scattering by cloud particles into account. Therefore, the authors conclude that their values could be overestimated by at least a factor of 2. Thus, we suggest that Encrenaz et al. (2004) could have overestimated their measured value of the CO mixing ratio in the stratosphere (external origin model) of Uranus and that scattering has a non negligible effect on the spectrum of Uranus at 4.7-μm. From our observations, there is no evidence of an external origin of CO. This molecule could be a good candidate for the production of the observed CO_2 (Burgdorf et al. 2006). Even if CO is not detected in our observations, the level of our upper limits does not imply that we should reconsider the possibility of production of CO_2 from CO, since CO_2 was detected at the $(4.0 \pm 0.5) \times 10^{-11}$ level. A complete photochemical model of Uranus, which takes chemical uncertainties into account (Hébrard et al. 2007; Hébrard et al. 2006; Dobrijevic et al. 2003) should be developed in order to test several hypothese for the supply of H_2O, CO_2 and CO in order to understand their chemistry and to model the observed abundances of these species.

6. Conclusion

Although this attempt to detect CO in the atmospheres of Saturn and Uranus has failed, new upper limits have been derived. Our upper limit on a CO internal source in the atmosphere of Saturn (3.9×10^{-8}, constant with altitude) is better than the previously published one (Rosenqvist et al. 1992) by a factor of 3. This upper limit on the internal source is far from the 1 ppb detection level of Noll & Larson (1991) and the upper limit we derived on the external source (6.3×10^{-8}, restricted to the stratosphere) is greater than the stratospheric abundance of CO in the external origin model of Noll & Larson (1991) (2.5×10^{-8}) by a factor of 2.5. New observations with higher sensitivity and/or more observing time should permit a derivation of the magnitude of the CO external source on Saturn. Our non-detection of CO at the 1.8×10^{-8} level in the atmosphere of Uranus is consistent with the latest published upper limit on an internal source of CO (2×10^{-8}, Encrenaz et al. 2004). Moreover, the upper limit we derived on the magnitude of an external source (2.7×10^{-8}, restricted to the stratosphere) is below the detection level of Encrenaz et al. (2004). However, our measurement is not incompatible with the result of Encrenaz et al. (2004) (3×10^{-8}, restricted to the stratosphere). Their fluorescence model did not take scattering effects by cloud particles into account. As a consequence, the mixing ratio they derived could have been overestimated. According to the authors, the uncertainty on their result could be at least a factor of 2. Moreover, our new upper limits add new constraints on the possible temporal variability of the abundance of CO in the atmospheres of these planets.

From our observations, it is still impossible to conclude on the strength of the external flux of oxygen in the atmosphere of Saturn and Uranus. This question could be answered by observing at higher frequency where the lines are stronger. Such observations would still need several hours of integration because of the sky opacity, which is higher at such frequencies. Such observations would be focused on the stratospheric narrow emission peak in order to derive the stratospheric CO abundance but could also be performed over a wide frequency range (Lellouch et al. 2005; Hesman et al. 2007). CO observations with the Herschel Space Observatory would also be very valuable with regard to its foreseen outstanding capability to detect faint lines in short integration times. Such observations should focus on the lines that have the strongest predicted line strength (good signal to noise ratio in a relatively short integration time) and for which

observations are independent of the ammonia and phosphine abundances (Cavalié et al. 2007).

References

Baines, K. H., Mickelson, M. E., Larson, L. E., & Ferguson, D. W. 1995, Icarus, 114, 328
Beaky, M. M., Goyette, T. M., & De Lucia, F. C. 1996, J. Chem. Phys., 105, 3994
Berge, G. L., & Gulkis, S. 1976, Earth-based radio observations of Jupiter: Millimeter to meter wavelengths, ed. T. Gehrels, 621
Bergin, E. A., Lellouch, E., Harwit, M., et al. 2000, ApJ, 539, L147
Bézard, B., Lellouch, E., Strobel, D., Maillard, J.-P., & Drossart, P. 2002, Icarus, 159, 95
Borysow, A., & Frommhold, L. 1986, ApJ, 304, 849
Borysow, J., Trafton, L., Frommhold, L., & Birnbaum, G. 1985, ApJ, 296, 644
Borysow, J., Frommhold, L., & Birnbaum, G. 1988, ApJ, 326, 509
Brown, L. R., & Peterson, D. B. 1994, J. Mol. Spec., 168, 593
Burgdorf, M., Orton, G., van Cleve, J., Meadows, V., & Houck, J. 2006, Icarus, 184, 634
Cavalié, T., Billebaud, F., Lellouch, E., et al. 2007, in Herschel Open time Key Program Workshop, 20−21 Feb. 2007, ESTEC, Noordwick, The Netherlands
Cavalié, T., Billebaud, F., Biver, N., et al. 2008, Planet. Space Sci., submitted
Conrath, B. J., & Gautier, D. 2000, Icarus, 144, 124
Conrath, B., Hanel, R., Gautier, D., Marten, A., & Lindal, G. 1987, J. Geophys. Res., 92, 15003
Coustenis, A., Salama, A., Lellouch, E., et al. 1998, A&A, 336, L85
Davis, G. R., Griffin, M. J., Naylor, D. A., et al. 1996, A&A, 315, L393
de Graauw, T., Feuchtgruber, H., Bezard, B., et al. 1997, A&A, 321, L13
de Pater, I., & Dickel, J. R. 1991, Icarus, 94, 474
Dobrijevic, M., Ollivier, J. L., Billebaud, F., Brillet, J., & Parisot, J. P. 2003, A&A, 398, 335
Draegert, D. A., & Dudley, W. 1968, J. Opt. Soc. Am., 58, 1399
Dunn, D. E., de Pater, I., Wright, M., Hogerheijde, M. R., & Molnar, L. A. 2005, AJ, 129, 1109
Encrenaz, T., Serabyn, E., & Weisstein, E. W. 1996, Icarus, 124, 616
Encrenaz, T., Lellouch, E., Drossart, P., et al. 2004, A&A, 413, L5
Feuchtgruber, H., Lellouch, E., de Graauw, T., et al. 1997, Nature, 389, 159
Feuchtgruber, H., Lellouch, E., Encrenaz, T., et al. 1999, in The Universe as Seen by ISO, ed. P. Cox, & M. Kessler, ESA Special Publication, 427, 133
Fletcher, L. N., Irwin, P. G. J., Teanby, N. A., et al. 2007, Icarus, 189, 457
Hébrard, E., Dobrijevic, M., Bénilan, Y., & Raulin, F. 2006, J. Photochem. Photobiol. C: Photochem. Rev., 7, 211
Hébrard, E., Dobrijevic, M., Bénilan, Y., & Raulin, F. 2007, Planet. Space Sci., 55, 1470
Hesman, B. E., Davis, G. R., Matthews, H. E., & Orton, G. S. 2007, Icarus, 186, 342
Hildebrand, R. H., Loewenstein, R. F., Harper, D. A., et al. 1985, Icarus, 64, 64
Hofstadter, M. D., & Muhleman, D. O. 1989, Icarus, 81, 396
Hunten, D. M. 1978, Nature, 276, 16
Klein, M. J., Janssen, M. A., Gulkis, S., & Olsen, E. T. 1978, Saturn's microwave spectrum: Implications for the atmosphere and the rings, ed. D. M. Hunten, & D. Morrison (NASA conference publ. 2068), 195
Lellouch, E. 1996, in The Collision of Comet Shoemaker-Levy 9 and Jupiter, ed. K. S. Noll, H. A. Weaver, & P. D. Feldman, IAU Colloq., 156, 213
Lellouch, E., Bézard, B., Moses, J. I., et al. 2002, Icarus, 159, 112
Lellouch, E., Moreno, R., & Paubert, G. 2005, A&A, 430, L37
Lévy, A., Lacome, N., & Tarrago, G. 1993, J. Mol. Spec., 157, 172
Lévy, A., Lacome, N., & Tarrago, G. 1994, J. Mol. Spec., 166, 20
Lindal, G. F. 1992, AJ, 103, 967
Marten, A., Gautier, D., Owen, T., et al. 1993, ApJ, 406, 285
Melnick, G., Russell, R. W., Gosnell, T. R., & Harwit, M. 1983, Icarus, 53, 310
Moreno, R. 1998, Ph.D. Thesis, AA (Université Paris VI)
Moses, J. I. 1996, in The Collision of Comet Shoemaker-Levy 9 and Jupiter, ed. K. S. Noll, H. A. Weaver, & P. D. Feldman, IAU Colloq., 156, 243
Moses, J. I., Lellouch, E., Bézard, B., et al. 2000, Icarus, 145, 166
Noll, K. S., & Larson, H. P. 1991, Icarus, 89, 168
Noll, K. S., Knacke, R. F., Geballe, T. R., & Tokunaga, A. T. 1986, ApJ, 309, L91
Ollivier, J. L., Dobrijévic, M., & Parisot, J. P. 2000, Planet. Space Sci., 48, 699
Orton, G. S., Griffin, M. J., Ade, P. A. R., Nolt, I. G., & Radostitz, J. V. 1986, Icarus, 67, 289
Orton, G. S., Baines, K. H., Bergstrahl, J. T., et al. 1987, Icarus, 69, 230
Pickett, H. M., Poynter, I. R. L., Cohen, E. A., et al. 1998, J. Quant. Spectr. Radiat. Transfer, 60, 883
Rosenqvist, J., Lellouch, E., Romani, P. N., Paubert, G., & Encrenaz, T. 1992, ApJ, 392, L99
Ulich, B. L. 1981, AJ, 86, 1619
Varanasi, P. 1988, J. Quant. Spectr. Radiat. Transfer, 39, 13
Wallace, L. 1980, Icarus, 43, 231
Weisstein, E. W., & Serabyn, E. 1996, Icarus, 123, 23